Title	Identification of Piecewise Linear Uniform Motion Blur
Authors	Karn Patanukhom, AKINORI NISHIHARA
Citation	IEICE Trans. Fundamentals, Vol. E91-A, No. 6, pp. 1416-1425
Pub. date	2008, 6
URL	http://search.ieice.org/
Copyright	(c) 2008 Institute of Electronics, Information and Communication Engineers

PAPER Special Section on Image Media Quality

Identification of Piecewise Linear Uniform Motion Blur

Karn PATANUKHOM[†a)], *Nonmember and* **Akinori NISHIHARA**[††], *Fellow*

SUMMARY A motion blur identification scheme is proposed for nonlinear uniform motion blurs approximated by piecewise linear models which consist of more than one linear motion component. The proposed scheme includes three modules that are a motion direction estimator, a motion length estimator and a motion combination selector. In order to identify the motion directions, the proposed scheme is based on a trial restoration by using directional forward ramp motion blurs along different directions and an analysis of directional information via frequency domain by using a Radon transform. Autocorrelation functions of image derivatives along several directions are employed for estimation of the motion lengths. A proper motion combination is identified by analyzing local autocorrelation functions of non-flat component of trial restored results. Experimental examples of simulated and real world blurred images are given to demonstrate a promising performance of the proposed scheme.

key words: *blur identification, motion blur, image restoration*

1. Introduction

Due to an imperfection of a recording process, in many practical situations, a recorded image is a degraded version of a desired original scene. For a noisy linear shift-invariant blur condition, the degradation process can be modeled in a spatial domain as

$$g(x, y) = h(x, y) * f(x, y) + n(x, y), \tag{1}$$

where $f(x, y)$ and $g(x, y)$ are original and blurred images, respectively; $n(x, y)$ is an additive noise; and $h(x, y)$ is called a point spread function (PSF) of the blur. One of well-known types of the image degradation is a motion blur. The motion blur is caused when there are relative motions between a camera and objects during exposure time. The motion blurred images are often seen when hand or camera is trembling, objects in the scene are moving, a light condition or shutter speed is low.

In general, a deblurring process can be considered as two problems that are identification and deconvolution problems. The first step of image restoration is to identify the PSF of blur and noise parameters. Then, to restore the original image, the blurred image is deconvoluted by using the estimated PSF of blur and noise parameters. Identification of the blur's PSF plays an important role in restoration of motion blurred images. To identify the motion blur, a number of approaches have been proposed [1]–[12]. The motion blurs can be identified by only using the information from blurred image itself which can be analyzed based on a zero-crossing pattern in transform domain [1], [2], an autocorrelation function of an image derivative [3], a trial restoration [4], [5], or human visual-motion sensing [6]. However, the identification ability of these methods are limited to a specific and very simple motion models such as linear motion in one direction or constant velocity of the motion. In some practical situations, the motion blur may not be a linear motion vector in a single direction. To identify more complex models of blurs, several methods such as auto-regressive (AR) model and maximum likelihood (ML) based methods [7], [8], vector quantization (VQ) based methods [9], [10] and multiple-image-based methods [11], [12], are proposed. Although these methods can be employed for more complex motion models, there are some practical limitations. ML-based approaches require a good prior estimation of the blur length, strong assumptions on image models, and high computational cost. For VQ-based approaches, there is a difficulty in selecting proper candidates of blur operator for blur identification codebook. Different shots of the scene are necessary in multiple-image-based methods which may require an additional hardware cost.

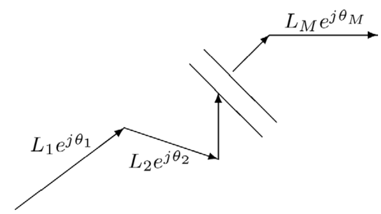

Fig. 1 Piecewise linear motion vector.

In this paper, a blur identification scheme for piecewise linear uniform motion blur (PLUMB) is proposed. The blur parameters are extracted from the blurred image itself without using any a priori knowledge of the original image or noise. The motion blur is approximated and considered to be a piecewise linear motion which has multiple directional components as shown in Fig. 1. The proposed scheme includes modules of a motion direction estimation, a motion length estimation, and a motion combination identification. A mathematical model for the PLUMB is described in Sect. 2. Details of the proposed scheme are presented

Manuscript received July 2, 2007.
Manuscript revised November 26, 2007.
[†]The author is with the Department of Communications and Integrated Systems, Tokyo Institute of Technology, Tokyo, 152-8552 Japan.
[††]The author is with the Center for Research and Development of Educational Technology, Tokyo Institute of Technology, Tokyo, 152-8552 Japan.
a) E-mail: karn@nh.cradle.titech.ac.jp
DOI: 10.1093/ietfec/e91–a.6.1416

in Sect. 3. Some experimental results are demonstrated in Sect. 4. Finally, Sect. 5 gives conclusions of this paper and directions for future work.

2. Piecewise Linear Uniform Motion Blur

The PSF of the linear motion blur with a constant velocity in a direction of θ for the length of L can be defined by

$$h(x, y; Le^{j\theta}) = h(x'_\theta, y'_\theta; L), \tag{2}$$

where

$$\begin{bmatrix} x'_\theta \\ y'_\theta \end{bmatrix} = \begin{bmatrix} \cos(\theta) & \sin(\theta) \\ -\sin(\theta) & \cos(\theta) \end{bmatrix} \begin{bmatrix} x \\ y \end{bmatrix}, \text{and} \tag{3}$$

$$h(x, y; L) = \begin{cases} 1/L; & 0 \le x \le L-1, y = 0, \\ 0; & \text{otherwise.} \end{cases} \tag{4}$$

For discrete spatial domain, interpolation techniques have to be employed for a rotation process in (3) when values of non-integer pixels are needed.

For the PLUMB, the motion shown in Fig. 1 is represented by a vector of linear motion components as

$$V = \begin{bmatrix} L_1 e^{j\theta_1} & L_2 e^{j\theta_2} & \dots & L_M e^{j\theta_M} \end{bmatrix}, \tag{5}$$

where V is a piecewise linear motion vector, θ_i and L_i are the motion direction and length of the i-th component; and M represents the number of motion components. The vector of motion direction, V_D, and the vector of motion length, V_L, are defined as

$$V_D = \begin{bmatrix} \theta_1 & \theta_2 & \dots & \theta_M \end{bmatrix}, \text{and} \tag{6}$$

$$V_L = \begin{bmatrix} L_1 & L_2 & \dots & L_M \end{bmatrix}. \tag{7}$$

From (5), V provides the information of motion directions and lengths of all piecewise linear components and an order of the combination to form its corresponding piecewise linear motion. Each element of V corresponds to each linear motion component which is represented by a complex number (in a polar form) where the motion length and direction are represented by amplitude and phase, respectively.

By assuming that the PSF has an uniform distribution of coefficients for an entire motion route which is identical to the constant motion velocity during an entire exposure period while the period for each linear motion becomes a direct variation of motion length, the PSF of PLUMB can be defined by

$$h(x, y; V) = \frac{1}{\sum_{i=1}^{M} L_i} \sum_{i=1}^{M} L_i h(x - X_i, y - Y_i; V_i), \tag{8}$$

where

$$X_i = \begin{cases} 0; & i = 1, \\ \displaystyle\sum_{k=1}^{i-1} L_k \cos(\theta_k); & \text{otherwise,} \end{cases} \tag{9}$$

$$Y_i = \begin{cases} 0; & i = 1, \\ \displaystyle\sum_{k=1}^{i-1} L_k \sin(\theta_k); & \text{otherwise,} \end{cases} \tag{10}$$

and $V_i = L_i e^{j\theta_i}$ is the i-th element of V. From (8), PSF for PLUMB model can be obtained by the weighted summation of the shifted versions of the PSFs of every linear motion component with constant velocity defined in (2). An example of PSF of PLUMB with $V_D = [-15° \ 30° \ 80°]$ and $V_E = [7 \ 7 \ 7]$ is illustrated in Fig. 7(b).

3. Proposed Scheme for PLUMB Identification

3.1 Identification Stages

To identify the PSF of PLUMB, the proposed three-stage scheme which consists of motion direction estimator, motion length estimator, and motion combination selector is demonstrated in Fig. 2. In Fig. 2, $\hat{\theta}_i$ and $\hat{L}_i$ represent estimated motion direction and length for the i-th motion component; $\hat{M}$ denotes the number of the identified motion components; and $\hat{h}(x, y)$ represents an estimated PSF of the blur. In the first stage, the directions of all motion components are identified. The result is a set of estimated motion direction, $\{\hat{\theta}_1, \hat{\theta}_2, \dots, \hat{\theta}_{\hat{M}}\}$. Note that $\hat{M}$ is also obtained in this stage. A proposed algorithm for the estimation of motion direction will be described in Sect. 3.2. Then, in the next stage, the motion length corresponding to each direction is estimated. As a result, a set of identified motion components, $\{\hat{L}_1 e^{j\hat{\theta}_1}, \hat{L}_2 e^{j\hat{\theta}_2}, \dots, \hat{L}_{\hat{M}} e^{j\hat{\theta}_{\hat{M}}}\}$, is obtained in this stage. Section 3.3 will present an algorithm to estimate the motion length for PLUMB. Although the set of motion components is estimated in the previous steps, the PSF from motion obtained by different ordering of the components affects the restored results. Therefore, it is important to choose the best combination. Section 3.4 will give details about how to choose the proper combination from the set of identified motion components.

3.2 Estimation of Motion Direction

The proposed scheme for motion direction estimation is based on the method of Tan, et al. [5]. In order to estimate the direction of the motion blur, Tan proposed to firstly try to restore the blurred image by using a forward ramp PSF

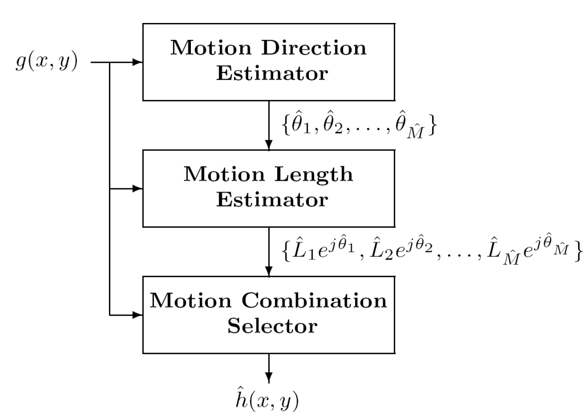

Fig. 2 Proposed three-stage identification scheme.

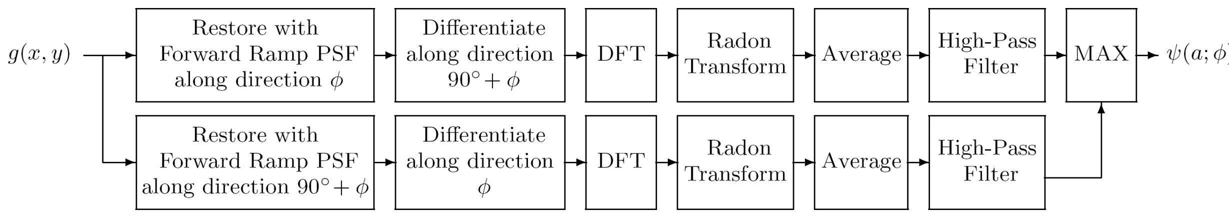

Fig. 3 Scheme for motion direction estimation.

along the horizontal direction. The PSF of the horizontal forward ramp motion blur with the length equal to L can be written by

$$h_{FR}(x, y; L) = \begin{cases} x+1; & 0 \le x \le L-1, y = 0, \\ 0; & \text{otherwise.} \end{cases} \tag{11}$$

Then, a vertical differentiation was applied to the trial restored image to strengthen strips along the blur direction. Finally, the image derivative was transformed into a Fourier domain; and a Radon transform was employed in the Fourier domain to extract an information about the direction. The expected motion direction was the direction corresponding to a location of maxima of the output after Radon transform. The method of Tan, however, did not consider the cases of multiple directional components.

In order to estimate a set of the motion directions for PLUMB, a direction analysis function ψ is defined as shown in Fig. 3. To compute ψ, the blurred image, $g(x, y)$, is firstly restored by using forward ramp PSF along the trial directions of ϕ and $90° + \phi$ with an arbitrary trial length, L_T. The PSF of the forward ramp motion blur in the directions of ϕ and $90° + \phi$ with the length of L_T can be obtained from

$$h_{FR}(x, y; L_T e^{j\theta}) = h_{FR}(x'_\theta, y'_\theta; L_T), \tag{12}$$

when $\theta = \phi$ and $90° + \phi$; and (x'_θ, y'_θ) is obtained from (3). The trial restored images are named as $\hat{f}_{FR}(x, y; \phi)$ and $\hat{f}_{FR}(x, y; 90° + \phi)$ for the directions of ϕ and $90° + \phi$, respectively. Then, the image differentiation along the directions of $90° + \phi$ and ϕ are applied to $\hat{f}_{FR}(\phi)$ and $\hat{f}_{FR}(90° + \phi)$, respectively, where the directional differentiation of any image $s(x, y)$ is calculated by

$$\Delta_\theta(s(x, y)) = s(x'_\theta, y'_\theta) - s(x'_\theta - 1, y'_\theta), \tag{13}$$

for any direction of θ; and (x'_θ, y'_θ) is obtained from (3). The image derivatives are denoted by $\Delta_{90°+\phi}(\hat{f}_{FR}(x, y; \phi))$ and $\Delta_\phi(\hat{f}_{FR}(x, y; 90° + \phi))$. A reason of using the parallel scheme of two perpendicular directions of ϕ and $90° + \phi$ is to strengthen the directional information of blur along the differentiation direction which may be lost due to the differentiation process. Then, the directional information is analyzed by using Fourier and Radon Transforms. $\Delta_{90°+\phi}(\hat{f}_{FR}(\phi))$ and $\Delta_\phi(\hat{f}_{FR}(90° + \phi))$ are transformed into DFT domain, resulting in $\mathcal{F}_1(\omega_x, \omega_y; \phi)$ and $\mathcal{F}_2(\omega_x, \omega_y; \phi)$, where ω_x and ω_y are horizontal and vertical frequencies, respectively. In order to extract the information about the direction, Radon transform is applied to $|\mathcal{F}_1(\omega_x, \omega_y; \phi)|$ and $|\mathcal{F}_2(\omega_x, \omega_y; \phi)|$. The Radon transform can be obtained by

$$\mathcal{R}_k(a, \rho; \phi) = \int_{-\infty}^{\infty}\int_{-\infty}^{\infty} [\, |\mathcal{F}_k(\omega_x, \omega_y; \phi)| \cdot \delta(\rho - \omega_x \cos(a) - \omega_y \sin(a))] d\omega_x d\omega_y, \tag{14}$$

where $k = 1$ and 2; $\mathcal{R}$ is the result after the Radon transform; a and ρ are the dimensions of an angle and a distance from the origin; respectively. Then, a local average of $\mathcal{R}_k(a, \rho; \phi)$ in the dimension of ρ denoted by $\bar{\mathcal{R}}_k(a; \phi)$ is calculated by

$$\bar{\mathcal{R}}_k(a; \phi) = \frac{1}{2D}\int_{-D}^{D} \mathcal{R}_k(a, \rho; \phi) d\rho, \tag{15}$$

where D is an adjusting parameter. Next, in order to emphasize the local maxima, a high-pass filtering operator is employed to $\bar{\mathcal{R}}_k(a; \phi)$ as

$$\tilde{\mathcal{R}}_k(a; \phi) = \bar{\mathcal{R}}_k(a; \phi) - \frac{1}{2A}\int_{-A}^{A} \bar{\mathcal{R}}_k(a; \phi) da, \tag{16}$$

where A is an adjusting parameter. Finally, ψ is defined by

$$\psi(a; \phi) = \max(\tilde{\mathcal{R}}_1(a; \phi), \tilde{\mathcal{R}}_2(a; \phi)). \tag{17}$$

Since, in practice, the motion directional information obtained from ψ are affected by ϕ used in trial restoration process, a scheme which uses multiple trial motion direction is preferable to cover more directional information. As a result, the set of motion direction can be obtained by applying the following iterative scheme.

Initialization: An initial identified set of motion directions denoted by $\{\hat{\theta}_1^{(0)}, \hat{\theta}_2^{(0)}, \ldots, \hat{\theta}_{\hat{M}^{(0)}}^{(0)}\}$ can be obtained from a set of locations of local maxima of $\Psi^{(0)}(a) = \psi(a; 0°)$ whose values are over a pre-determined threshold.

Updating: The identified set of motion directions in the p-th iteration, $\{\hat{\theta}_1^{(p)}, \hat{\theta}_2^{(p)}, \ldots, \hat{\theta}_{\hat{M}^{(p)}}^{(p)}\}$, is the set of locations of local maxima of $\Psi^{(p)}(a)$ whose values are over a threshold where

$$\Psi^{(p)}(a) = \max_i(\psi(a; \hat{\theta}_i^{(p)}), \Psi^{(p-1)}(a)). \tag{18}$$

The iteration can be terminated when the difference between $\{\hat{\theta}_1^{(p)}, \hat{\theta}_2^{(p)}, \ldots, \hat{\theta}_{\hat{M}^{(p)}}^{(p)}\}$ and $\{\hat{\theta}_1^{(p-1)}, \hat{\theta}_2^{(p-1)}, \ldots, \hat{\theta}_{\hat{M}^{(p-1)}}^{(p-1)}\}$ is small enough.

3.3 Estimation of Motion Length

The proposed motion length estimation scheme is modified from the method of Yitzhaky [3]. Yitzhaky proposed that the motion length can be estimated from a location of global minima of an autocorrelation function (ACF) extracted from

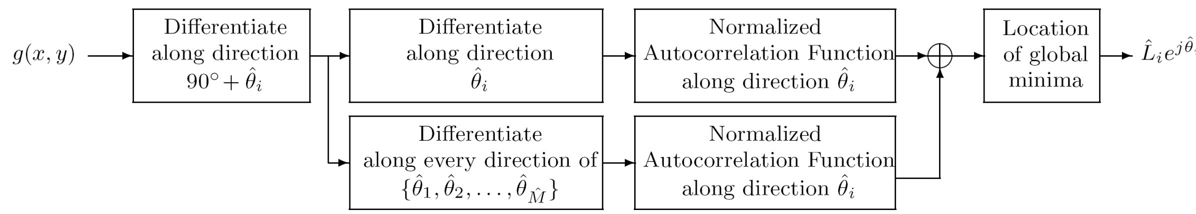

Fig. 4 Scheme for motion length estimation.

an image derivative along the motion direction. However, an identification accuracy of this method is low when it is extended to use for PLUMB.

To improve the identification results, the modified scheme is proposed as shown in Fig. 4. Since, in the cases of PLUMB, there is more than one directional component, the identification of the motion length for each component may be interfered by other components. As a result, the scheme is modified by adding a lower path illustrated in Fig. 4 which is differentiation along every identified motion direction to reduce the effect from the other directional components. For estimation of the blur length along the direction of $\hat{\theta}_i \in \{\hat{\theta}_1, \hat{\theta}_2, \ldots, \hat{\theta}_{\hat{M}}\}$ which is denoted by $\hat{L}_i$, the differentiation of the blurred image, $g(x, y)$, along directions of $90^\circ + \hat{\theta}_i$ and $\hat{\theta}_i$ are continuously computed where the output is named as $\Delta_S(g(x, y); \hat{\theta}_i)$. In parallel, the image differentiation along directions of $90^\circ + \hat{\theta}_i, \hat{\theta}_1, \hat{\theta}_2, \ldots$, and $\hat{\theta}_{\hat{M}}$ are also applied to the blurred image, continuously; and the result is denoted by $\Delta_A(g(x, y); \hat{\theta}_i)$. Then, the normalized ACFs along the direction of $\hat{\theta}_i$ are computed for $\Delta_S(g; \hat{\theta}_i)$ and $\Delta_A(g; \hat{\theta}_i)$, resulting in $R_S(\tau; \hat{\theta}_i)$ and $R_A(\tau; \hat{\theta}_i)$, respectively. After that, $R_S(\tau; \hat{\theta}_i)$ and $R_A(\tau; \hat{\theta}_i)$ are added together to obtain $R_T(\tau; \hat{\theta}_i)$. Finally, the identified blur length for the direction of $\hat{\theta}_i$ is a location of the global minima of $R_T(\tau; \hat{\theta}_i)$. After the process has been repeated for every direction of $\hat{\theta}_i$ where $i = 1, 2, \ldots, \hat{M}$, in the end of this stage, the set of identified motion components, $\{\hat{L}_1 e^{j\hat{\theta}_1}, \hat{L}_2 e^{j\hat{\theta}_2}, \ldots, \hat{L}_{\hat{M}} e^{j\hat{\theta}_{\hat{M}}}\}$, is obtained.

3.4 Identification of Motion Combination

Although the set of motion directions and lengths can be estimated by the methods proposed in Sects. 3.2 and 3.3, the ordering of the motion components to form the piecewise linear motion vector is still the other parameter that have to be identified. In this work, to limit the number of possible combinations, we assume that the actual motion directions are mutually different from each other or $\theta_i \neq \theta_j$ when $i \neq j$. Then, in order to select the proper combinations of the motion vector, we propose the following steps.

Step 1: By using an identified set of the motion components, $\{\hat{L}_1 e^{j\hat{\theta}_1}, \hat{L}_2 e^{j\hat{\theta}_2}, \ldots, \hat{L}_{\hat{M}} e^{j\hat{\theta}_{\hat{M}}}\}$, obtained in Sects. 3.2 and 3.3, the motion components are permutated to create all possible PSFs where the PSF of the q-th permuted combination is denoted by $\hat{h}_q(x, y)$. The number of all PSFs, N_C, is equal to $2^{\hat{M}-1}\hat{M}!$ obtained from $\hat{M}!$ possible cases that can be permuted from $\hat{M}$ components and two cases for forward and reverse directions ($\hat{\theta}_i$ and $180^\circ + \hat{\theta}_i$) which provide the same identified result for $\hat{M} - 1$ components (one component is used for reference).

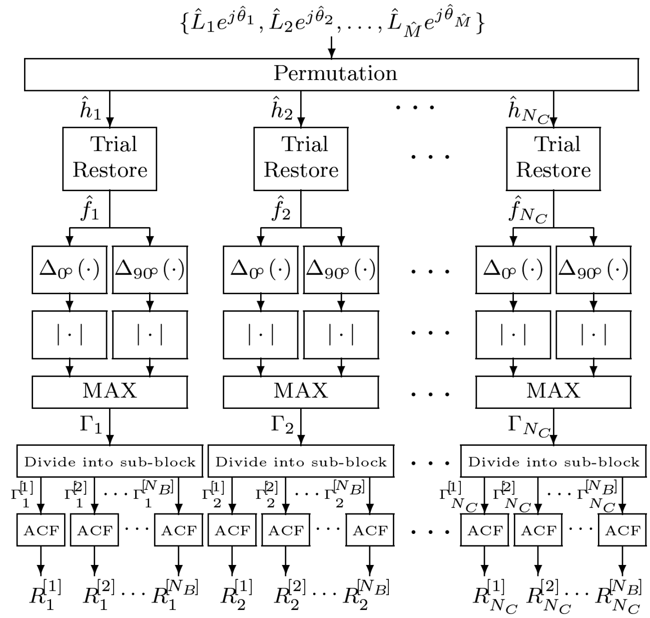

Fig. 5 Scheme for motion combination identification.

Step 2: The blurred image, $g(x, y)$, is restored on trial by using every possible $\hat{h}_q(x, y)$, resulting in $\hat{f}_q(x, y)$ when $1 \leq q \leq N_C$.

Step 3: To evaluate the trial restored results, the image derivatives in both horizontal and vertical directions are computed for every $\hat{f}_q(x, y)$, resulting in $\Delta_{0^\circ}(\hat{f}_q(x, y))$ and $\Delta_{90^\circ}(\hat{f}_q(x, y))$, respectively.

Step 4: A non-flat component, $\Gamma_q(x, y)$, is given by

$$\Gamma_q(x, y) = \max(|\Delta_{0^\circ}(\hat{f}_q(x, y))|, |\Delta_{90^\circ}(\hat{f}_q(x, y))|). \qquad (19)$$

Step 5: Each Γ_q is divided into N_B sub-blocks, resulting in $\Gamma_q^{[r]}$ for $1 \leq r \leq N_B$. A normalized ACF of $\Gamma_q^{[r]}$ denoted as $R_q^{[r]}$ is computed by

$$R_q^{[r]}(x, y) = \frac{\sum_{m_x, m_y} \Gamma_q^{[r]}(m_x, m_y)\Gamma_q^{[r]}(m_x - x, m_y - y)}{\sum_{m_x, m_y} \Gamma_q^{[r]}(m_x, m_y)\Gamma_q^{[r]}(m_x, m_y)}. \qquad (20)$$

A diagram for the step one to five is shown in Fig. 5.

Step 6: Under an assumption that good restoration results should have less residual blur and ringing artifact which corresponds to less spread in the ACF, the spread of ACF is compared by observing an area size of ACF whose value is over a threshold level. As a result, *Area* and *Size* functions are calculated by

$$Area_q^{[r]}(x,y) = \begin{cases} 0; & R_q^{[r]}(x,y) < T, \\ 1; & R_q^{[r]}(x,y) \geq T, \end{cases} \tag{21}$$

$$Size_q^{[r]} = \sum_{x,y} Area_q^{[r]}(x,y), \tag{22}$$

where T is the threshold level. To determine the spread of the ACFs, a binary quantization is applied to the normalized ACF, resulting in *Area* function. Then, in order to compare the spread of ACF, the size of area is counted form the *Area* function where $Area_q^{[r]}(x,y) = 1$. The threshold level, T, in (21) can be arbitrary but must be the same value for every trial restored version for comparison. However, T which provides higher variation of $Size_q^{[r]}$ with respect to q is preferable in the next step for more obvious comparison of the spread of ACF between trial restored results.

Step 7: In order to compare the spread of ACF, *Score* function and *TotalScore* function are calculated by

$$Score_q^{[r]} = \begin{cases} 1; & Size_q^{[r]} \leq Size_k^{[r]} \text{ for } 1 \leq k \leq N_C, \\ 0; & \text{otherwise}, \end{cases} \tag{23}$$

$$TotalScore(q) = \sum_{r=1}^{N_B} Score_q^{[r]}. \tag{24}$$

In every sub-block, the *Size* function between the trial restored versions are compared and a score is given to the trial restored version that provides the minimum value of *Size* function comparing to the other trial restored version as shown in (23). Then, a summation of the *Score* function for every trial restored image is calculated as (24), resulting in *TotalScore* function. Finally, the identified PSF is $\hat{h}_q(x,y)$ which gives the maximum $TotalScore(q)$.

4. Experimental Results

In this section, the performance of the proposed method is presented for both simulation and real world cases in Sects. 4.1 and 4.2, respectively. In every simulation, the blurred images were added with Gaussian noise, resulting in $SNR = 40$ dB. The proposed method was used to identify the motion blurred images for the identification step. After the PSF is estimated, the blurred image is deconvoluted by using a method based on [13]. There is an example given to demonstrate the details of each stage of the proposed identification scheme in comparison to the conventional approaches.

4.1 Simulated Blur

Experiment I: The first example is the PLANE image with the size of 512×512 shown in Fig. 6. The original image

Fig. 6 Original PLANE image.

(a) Noisy Blurred Image

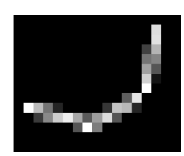

(b) PSF

Fig. 7 Noisy motion blurred version of PLANE image with V_D= [$-15°$ $30°$ $80°$] and V_E = [7 7 7] and SNR = 40 dB.

is blurred by the simulated PSF with V_D = [$-15°$ $30°$ $80°$] and V_L = [7 7 7] illustrated in Fig. 7(b). The noisy blurred version is shown in Fig. 7(a).

The results of the motion direction estimation are demonstrated in Fig. 8. The output of Radon transform, $\mathcal{R}_1(a,\rho;0°)$, which is used to identify the motion direction in the conventional method [5] is shown in Fig. 8(a). The directions of three motion components can not clearly be observed from $\mathcal{R}_1(a,\rho;0°)$. On the other hand, Fig. 8(b) shows the parameter Ψ (normalized by the maximum value) which is used in the proposed scheme for both $\Psi^{(0)}(a)$ (initial iteration) and $\Psi^{(1)}(a)$ (final iteration). The identification result is obtained from the locations of local maxima whose value are over the threshold level that was empirically chosen as 0.3 of the maximum value which provides good performances for the most of testing images and PSFs based on the experiment. From Fig. 8, the estimated sets of motion directions are $\{41°, 79°, 135°, 172°\}$ in the initial iteration and $\{41°, 80°, 172°\}$ in the final iteration (172° is equivalent to $-8°$). From the results, the directions of three motion components can be clearly observed by using the proposed scheme via the parameter Ψ. In addition, the iteration process can provide the result that is closer to actual set of motion directions which is $\{-15°, 30°, 80°\}$ in this example.

The proposed estimation of motion lengths via the ACF, $R(\tau; \hat{\theta}_i)$, for the directions of $\theta_i \in \{41°, 80°, 172°\}$ is presented in Fig. 9 for both the proposed and conventional schemes [3]. The conventional approach gives the identified lengths (locations of global minimum) which are equal to 5, 9, and 10 for the directions of 41°, 80°, and 172°, respectively. On the other hand, the proposed method gives the identified lengths of 5, 8, and 6 for the directions of 41°, 80°, and 172°, respectively. The identification results obtained from the proposed method are closer to the actual vector of motion length which is equal to [7 7 7] than the conventional method.

Figure 10(a) shows 24 possible combinations permuted from three identified motion components, $\{5e^{\frac{41}{180}j\pi}, 8e^{\frac{80}{180}j\pi}, 6e^{\frac{172}{180}j\pi}\}$, obtained in two previous stages. All PSFs in 10(a) have the same identified motion lengths and directions (forward and reverse) but only the order of combinations are different. Figure 10(b) shows *TotalScore* functions used for choosing the proper combination. The identification result is the 14th-combination ($\hat{V} = [6e^{\frac{-8}{180}j\pi}\ 5e^{\frac{41}{180}j\pi}\ 8e^{\frac{80}{180}j\pi}]$) whose *TotalScore* is the highest which can be observed from Fig. 10(b).

In this example, the proposed scheme is programmed by MATLAB7 and tested on a machine with Pentium D Processor 3.00 GHz and RAM 2.00 GB. An actual computational time that is needed to identify the blur is about 250 sec.

Finally, the restored result obtained by deconvoluting the blurred image with the identified PSF (14th-combination in Fig. 10(a)) is demonstrated in Fig. 11.

Experiment II: This experiment is conducted to compare the performance of blur direction identification by the proposed and conventional schemes [5]. Since the conventional scheme does not consider the multiple directional component, the comparison is done by using the linear motion blur with constant velocity model. The original PLANE image in Fig. 6 is blurred by a linear motion blur with length of nine where the motion direction, θ, is varied from 0° to 180°. The identified direction, $\hat{\theta}$, is obtained by the proposed and conventional schemes and the identification er-

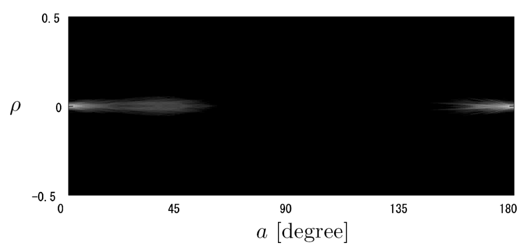

(a) Conventional Approach

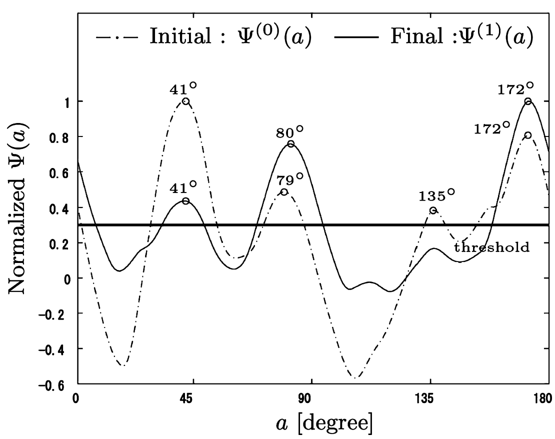

(b) Proposed Approach

Fig. 8 Estimation of motion direction for Fig. 7(a).

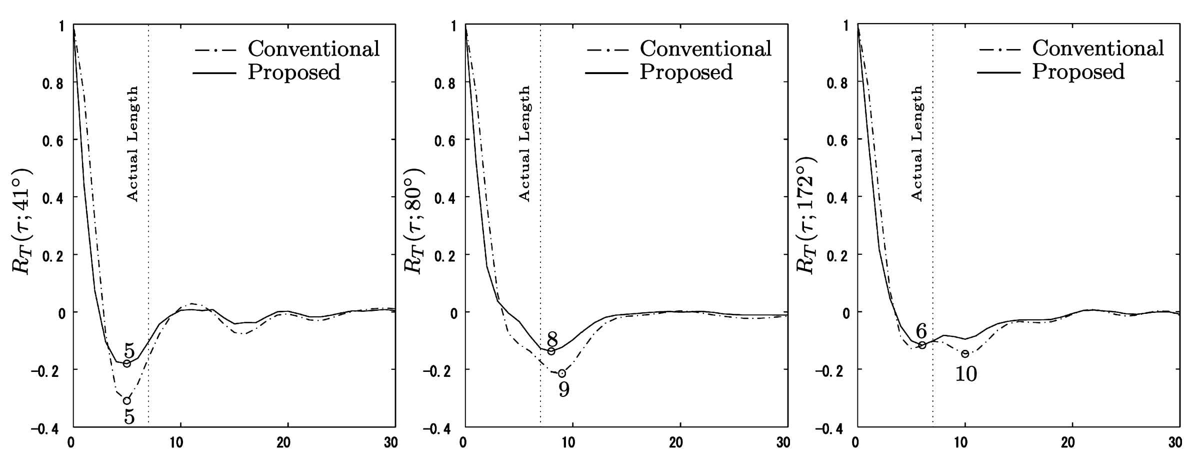

(a) $\hat{\theta}_1 = 41°$ (b) $\hat{\theta}_2 = 80°$ (c) $\hat{\theta}_3 = 172°$

Fig. 9 Estimation of motion length for Fig. 7(a).

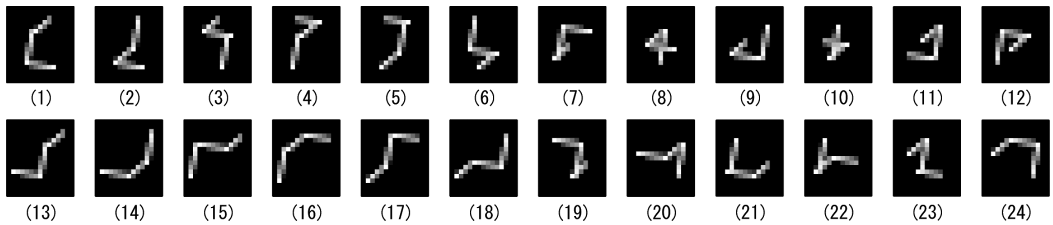

(a) Possible Motion Combinations (from the Set of Identified Components = $\{5e^{\frac{41}{180}j\pi}, 8e^{\frac{80}{180}j\pi}, 6e^{\frac{172}{180}j\pi}\}$)

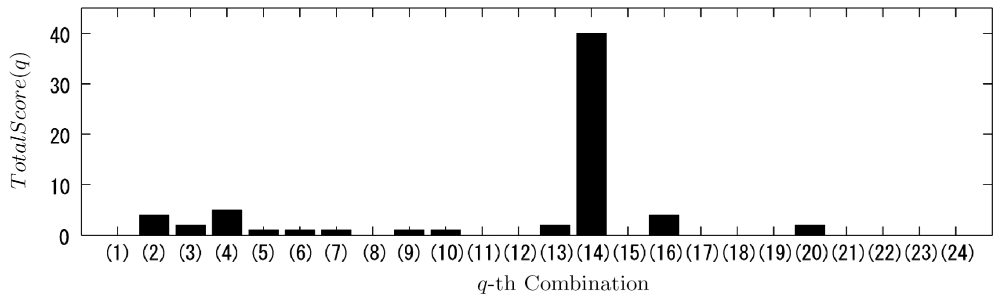

(b) *TotalScore* Function

Fig. 10 Identification of motion combination of Fig. 7(a).

Fig. 11 Restored image of Fig. 7(a).

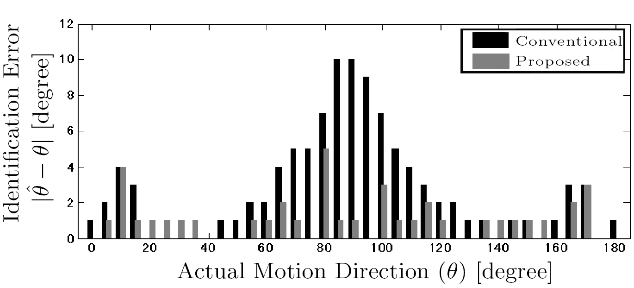

Fig. 12 Motion direction estimation of linear motion blur in various direction.

rors, $|\hat{\theta} - \theta|$, are calculated. A distribution of the errors is demonstrate in Fig. 12. The identification error obtained from the conventional scheme is higher around the vertical direction due to the effect of vertical differentiation while the proposed scheme using multiple trial direction, ϕ, can provide more uniform error and reduce a mean of identification error from 2.7778° to 1.1111°.

Experiment III: The effectiveness of the proposed modified scheme for estimation of motion length comparing to the conventional scheme [3] is presented in this experiment. The original PLANE image in Fig. 6 is blurred by twelve simulated PSFs in the PLUMB model. The lists of the original motion vector, identified motion lengths, $\hat{V}_L$, and their corresponding identification errors, $|\hat{V}_L - V_L|$, are shown in Table 1. An average of identification error per directional component is calculated from twelve samples that include totally 32 directional components. The identification results show that the proposed modified scheme can reduce the average identification error from 1.2188 to 0.6875.

Experiment IV: In this sub-section, the proposed scheme was used to identify simulated blurred images with different original images and PSFs. The blurred images were deconvoluted by identified PSFs. The restoration results were evaluated via improvement in signal to noise ratio, *ISNR*, which is defined by

$$ISNR = PSNR_{\hat{f}} - PSNR_g, \tag{25}$$

where $PSNR_s$ for $s(x, y) = g(x, y)$ and $\hat{f}(x, y)$ is obtained by

$$PSNR_s = 10 \log \left[\frac{255^2 N_x N_y}{\sum_{x,y}(s(x, y) - f(x, y))^2} \right], \tag{26}$$

for image size of $N_x \times N_y$. The identified vectors of motion directions and lengths ($\hat{V}_D$ and $\hat{V}_L$) and their corresponding *PSNR* and *ISNR* of several blurred images are demonstrated in Table 2. The results show that the proposed method was successful to estimate vectors of direction and length well and gave the good restoration results which can be observed via *ISNR*.

Table 1 Motion length estimation of PLANE image with various PSFs.

Actual Motion Vector		Estimated Motion Lengths			
		Conventional [3]		Proposed	
V_D	V_L	$\hat{V}_L$	$\lvert\hat{V}_L - V_L\rvert$	$\hat{V}_L$	$\lvert\hat{V}_L - V_L\rvert$
[0° 30°]	[5 9]	[7 11]	[2 2]	[6 10]	[1 1]
[0° 60°]	[5 9]	[5 10]	[0 1]	[5 10]	[0 1]
[0° 90°]	[5 9]	[5 9]	[0 0]	[5 9]	[0 0]
[0° 120°]	[5 9]	[5 10]	[0 1]	[5 9]	[0 0]
[0° 150°]	[5 9]	[5 9]	[0 0]	[5 9]	[0 0]
[0° 45° 90°]	[10 5 7]	[11 4 8]	[1 1 1]	[10 3 7]	[0 2 0]
[0° 45° 90°]	[7 4 4]	[8 4 5]	[1 0 1]	[7 4 4]	[0 0 0]
[60° −20° 30°]	[7 7 7]	[4 10 6]	[3 3 1]	[5 9 7]	[1 1 1]
[−20° 30° 80°]	[7 7 7]	[9 6 8]	[2 1 1]	[8 6 8]	[1 1 1]
[70° 140° 180°]	[7 5 9]	[9 4 10]	[2 1 1]	[9 4 9]	[2 1 0]
[45° 160° −90°]	[11 5 5]	[13 6 7]	[2 1 2]	[13 6 7]	[2 1 2]
[90° 45° 0° −45°]	[5 6 9 4]	[6 4 4 4]	[1 2 5 0]	[5 4 8 4]	[0 2 1 0]
Average Error per Directional Component		1.2188		0.6875	

Table 2 Identification and restoration results by using proposed scheme.

Image (512 × 512)	Actual Motion Vector		Estimated Motion Vector		$PSNR$ [dB]		$ISNR$ [dB]
	V_D	V_L	$\hat{V}_D$	$\hat{V}_L$	g	$\hat{f}$	
PLANE	[45° −30°]	[9 9]	[45° −29°]	[9 9]	22.9206	34.9134	11.9928
	[−15° 30° 80°]	[7 7 7]	[−8° 41° 80°]	[6 5 8]	21.5258	28.0485	6.5227
	[70° 140° 180°]	[10 5 7]	[71° 136° 178°]	[11 4 6]	21.2408	29.5017	8.2609
LENNA	[−30° 50°]	[11 11]	[−35° 48°]	[12 11]	21.4409	25.5173	4.0764
	[120° 40° 0°]	[9 5 7]	[116° 44° 2°]	[11 5 9]	20.6011	26.3715	5.7704
	[10° 50° 140°]	[7 10 9]	[16° 48° 136°]	[5 11 10]	20.8873	25.5545	4.6672
PEPPERS	[120° 15°]	[8 11]	[118° 15°]	[9 11]	22.7087	28.5113	5.8026
	[10° 50°]	[9 5]	[9° 47°]	[10 5]	24.5400	30.2049	5.6649
	[0° 80° 40°]	[9 5 4]	[−1° 84° 47°]	[9 6 3]	24.1867	28.3024	4.1157
BOAT	[5° 105°]	[6 10]	[8° 103°]	[7 10]	20.8253	31.5510	10.7257
	[−75° 75°]	[7 8]	[−75° 73°]	[8 8]	23.7790	28.9861	5.2071
	[−90° −45° 45°]	[5 5 4]	[−89° −47° 47°]	[5 4 4]	21.9204	31.2507	9.3303

4.2 Real World Blur

In this sub-section, the identification result of a sample real world blurred image obtained by using the proposed scheme and its corresponding restored result are demonstrated. Figure 13 shows an original real world blurred image with the size of 480 × 640. The result from each identification process is given in Fig. 14. From Fig. 14(a), the estimated set of directions is obtained as $\{13°, 92°\}$. Figure 14(b) shows that the identified lengths which are equal to 11 and 3 in the directions of 13° and 92°, respectively. The combination estimation process which consists of PSFs of four possible combinations permuted from two identified components and *TotalScore* function obtained from each combination is illustrated in Fig. 14(c). Finally, the identified motion combination is the second PSF in Fig. 14(c) whose $\hat{V}_D = [13°\ 92°]$ and $\hat{V}_L = [11\ 3]$. Then, the corresponding restored image is illustrated in Fig. 15. The characters appearing in the image can clearly be seen in the restored image in comparison to the original blurred image in Fig. 13. By using the same

Fig. 13 Real world blurred image.

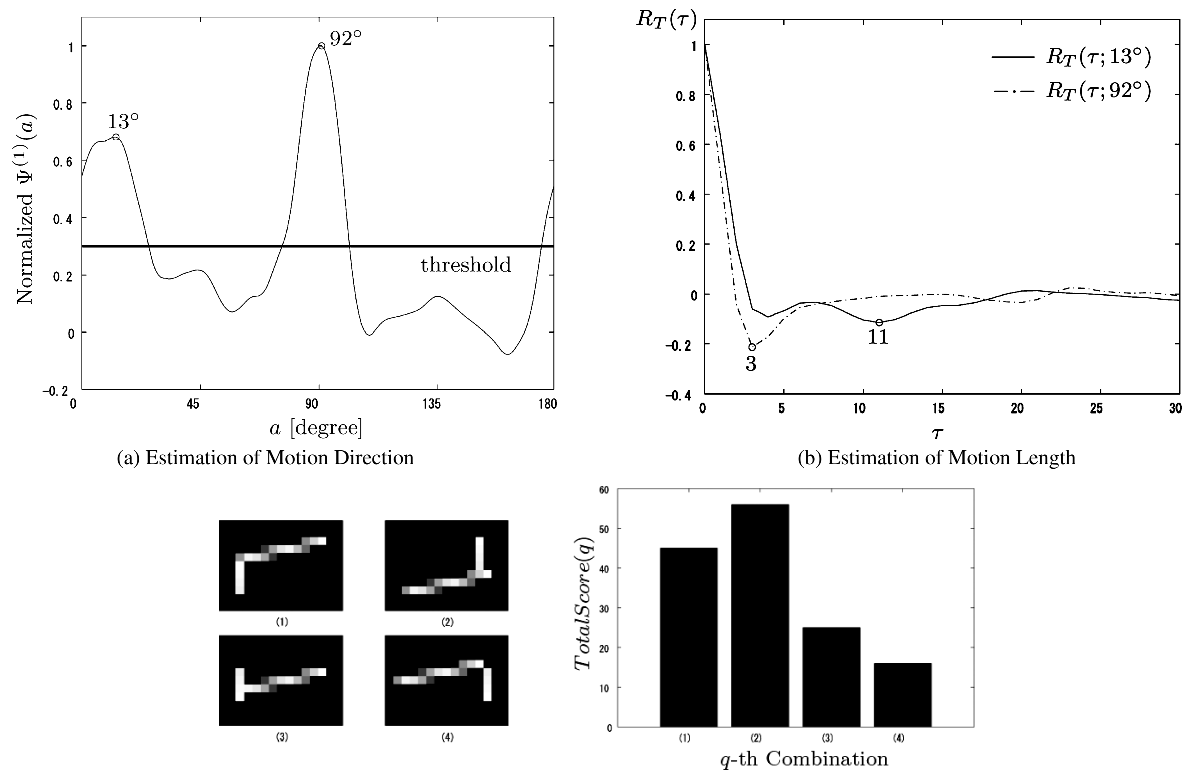

(a) Estimation of Motion Direction

(b) Estimation of Motion Length

(c) Identification of Motion Combination

Fig. 14 Details of identification process for Fig. 13.

Fig. 15 Restored image for Fig. 13.

machine mentioned in the previous example, it took about 150 sec. in this example.

5. Conclusion

The single image based scheme for identifying the PSF of PLUMB without using any information about the original image and noise was proposed. The proposed scheme consists of the algorithms for the motion direction and length estimation and the motion combination identification. The experiment demonstrated that the proposed scheme provides the ability to estimate the PSF of PLUMB in the both cases of simulation and real world blurred images and provides the better performances, comparing to the conventional methods. Although the number of linear motion components of the blurs is expected to be small in many practical situations, the computational cost of the proposed scheme exponentially increases with the increase in the the number of motion components; therefore, it is difficult to identify the blur with a large number of motion components. For the future work, the performance of the proposed scheme should be improved in the cases when there is a large number of components, or the direction of component is too close to each others or in the same direction.

References

[1] D.B. Gennery, "Determination of optical transfer function by inspection of frequency-domain plot," J. Optical Society of America, vol.63, no.12, pp.1571–1577, Dec. 1973.

[2] Y. Yoshida, K. Horike, and K. Fujita, "Parameter estimation of uniform image blur using DCT," IEICE Trans. Fundamentals, vol.E76-A, no.7, pp.1154–1157, July 1993.

[3] Y. Yitzhaky and N.S. Kopeika, "Identification of blur parameters from motion blurred images," CVGIP: Graphical models and image processing, vol.59, no.5, pp.310–320, Sept. 1997.

[4] Y. Jianchao, "Motion blur identification based on phase change ex-

perienced after trial restorations," 1999 IEEE Inter. Conf. on Image Processing, vol.1, pp.180–184, Oct. 1999.

[5] W. Tan, J. Zhang, G. Rong, and H. Chen, "Identification of motion blur direction based on analysis of intentional restoration errors," 2004 IEEE Inter. Conf. on Networking, Sensing and Control, vol.2, pp.1253–1258, 2004.

[6] Y. Chen and I. Choa, "An approach to estimating the motion parameters for a linear motion blurred image," IEICE Trans. Inf. & Syst., vol.E83-D, no.7, pp.1601–1603, July 2000.

[7] A.K. Katsaggelos and K.T. Lay, "Maximum likelihood blur identification and image restoration using the EM algorithm," IEEE Trans. Signal Process., vol.39, no.3, pp.729–733, March 1991.

[8] M.A.T. Figueriredo and R.D. Nowak, "An EM algorithm for wavelet-based image restoration," IEEE Trans. Image Process., vol.12, no.8, pp.906–916, Aug. 2003.

[9] K. Panchapakesan, D.G. Sheppard, M.W. Marcellin, and B.R. Hunt, "Blur identification from vector quantizer encoder distortion," IEEE Trans. Image Process., vol.10, no.3, pp.465–470, March 2001.

[10] R. Nakagaki and A.K. Katsaggelos, "A VQ-based blind image restoration algorithm," IEEE Trans. Image Process., vol.19, no.9, pp.1024–1053, Sept. 2003.

[11] M. Ben-Ezra and S.K. Nayar, "Motion-based motion deblurring," IEEE Trans. Pattern Anal. Mach. Intell., vol.26, no.6, pp.689–698, June 2004.

[12] M. Tico, M. Trimeche, and M. Vehvilainen, "Motion blur identification based on differently exposed images," IEEE International Conference on Image Processing, 2006, pp.2021–2024, Oct. 2006.

[13] L. Liang and Y. Xu, "Adaptive landweber method to deblur images," IEEE Trans. Signal Process., vol.10, no.5, pp.129–132, May 2003.

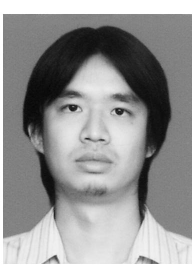

Karn Patanukhom was born in 1981. He received the B. Eng. degree in Electrical Engineering from Chiang Mai University in 2003, and the M. Eng. degree from Tokyo Institute of Technology in 2006. Since 2006 he has been working toward the Ph.D. degree at the Tokyo Institute of Technology. His research interest is in image processing, especially in image restoration problem.

Akinori Nishihara received the B.E., M.E. and Dr. Eng. degrees in electronics from Tokyo Institute of Technology in 1973, 1975 and 1978, respectively. Since 1978 he has been with Tokyo Institute of Technology, where he is now Professor of the Center for Research and Development of Educational Technology. His main research interests are in one- and multi-dimensional signal processing, and its application to educational technology. He has published more than 200 technical papers in international journals and conferences. He served as an Associate Editor of the IEICE Transactions on Fundamentals of Electronics, Communications and Computer Sciences from 1990 to 1994, and then an Associate Editor of the Transactions of IEICE Part A (in Japanese) from 1994 to 1998. He was an Associate Editor of the IEEE Transactions on Circuits and Systems II from 1996 to 1997 and Editor-in-Chief of Transactions of IEICE Part A (in Japanese) from 1998 to 2000. He served in IEEE Region 10 Executive Committee in various positions, and the Executive Committee of IEEE Tokyo Section and IEEE Japan Council for the last 10 years. He was a member of the Board of Governors, IEEE Circuits and Systems Society (2004–2005), and was Chair of IEEE Circuits and Systems Society Japan Chapter (2006–2007). He was Chair of the IEICE Technical Group on Circuits and Systems from 1997 to 1998, and since 1998 he has been serving as an Adviser of that Technical Group. He is now serving as IEICE Director, Conferences, Student Activities, and Education. He received a Best Paper Award of the IEICE in 1999, and IEEE Third Millennium Medal in 2000. He also received a Distinguished Service Award for IEEE Student Activities in 2006. Prof. Nishihara is a Fellow of IEEE, and a member of EURASIP, European Circuits Society, and Japan Society for Educational Technology.